NUCL SCI TECH (2016) 27:105
DOI 10.1007/s41365-016-0108-4

Iterative and accurate determination of small angle X-ray scattering background

Geng Wang[1,2,3] · Li-Feng Xu[3,4] · Jian-Lei Shen[3,4] · Guang-Bao Yao[3,4] · Zhi-Lei Ge[3,4] · Wen-Qin Li[1] · Chun-Hai Fan[1,3,4] · Gang Chen[1,2,3]

Received: 11 April 2016 / Revised: 4 June 2016 / Accepted: 7 June 2016 / Published online: 24 August 2016

Abstract X-ray scattering is widely used in material structural characterizations. The weak scattering nature, however, makes it susceptible to background noise and can consequently render the final results unreliable. In this paper, we report an iterative method to determine X-ray scattering background and demonstrate its feasibility by small angle X-ray scattering on gold nanoparticles. This method solely relies on the correct structural modeling of the sample to separate scattering signal from background in data fitting processes, which allows them to be immune from experimental uncertainties. The importance of accurate determination of the scaling factor for background subtraction is also illustrated.

Keywords X-ray scattering background · SAXS · Gold nanoparticles

This work was supported by the National Natural Science Foundation of China (No. 11375256) and the Science and Technology Commission of Shanghai Municipality (No. 14JC1493300).

✉ Gang Chen
gchen@shanghaitech.edu.cn

[1] Shanghai Synchrotron Radiation Facility, Shanghai Institute of Applied Physics, Chinese Academy of Sciences, Shanghai 201204, China

[2] School of Physical Science and Technology, ShanghaiTech University, Shanghai 201210, China

[3] CAS Key Laboratory of Interfacial Physics and Technology, Shanghai Institute of Applied Physics, Chinese Academy of Sciences, Shanghai 201204, China

[4] Division of Physical Biology, Shanghai Institute of Applied Physics, Chinese Academy of Sciences, Shanghai 201800, China

1 Introduction

With the advent of modern synchrotron radiation sources and the prevalence of nanotechnology, X-ray scattering technique capable of yielding structural details at the length scale of nanometer and beyond has been widely used in a variety of research fields, such as structural biology [1, 2], colloidal science [3–5] and polymer physics [6, 7]. It is proven to be one of the most powerful structural characterization techniques. In contrast to the complexity of data reduction for light scattering with lasers as a consequence of multiple scatterings [8], X-rays interact weakly with matters and thus provide a relatively simple path to the knowledge of particle sizes, shapes, etc. However, the intensity of X-ray scattering decreases rapidly with wavevector transfer and falls quickly into the level of scattering background. A proper way to handle this background is crucial for accurate structural determination, as any miscalculation would affect greatly the net scattering intensity and the final results.

X-ray scattering background can be divided into two categories: inherent (incoherent scattering, sample compressibility) and external to the sample (environmental background, scattering from sample holders, etc.). The background is usually handled by doing two separate experiments: with and without samples under the same experimental conditions [9–11]. The first experiment records X-ray scattering intensity (I_b), which composes of the scattering signal from samples and the background. The second experiment is done for subtracting the background scattering (I_b) from I_{sb}, so as to obtain the net scattering intensity I_s (X-ray scattering intensity from the sample itself)

$$I_s = I_{sb} - r_{bg} I_b, \quad (1)$$

where r_{bg} is the scaling factor. The conventional method to obtain r_{bg} is to measure the ratio between the attenuated fluxes of the direct beam under the same conditions through the sample holder with and without samples inside it [12–14]. This requires two ionization chambers installed directly in front and back of the sample, as shown in Fig. 1. However, gases filled in the ionization chambers bring additional background scattering and produce parasitic scattering. Also, instability of the incident X-ray beam will influence the accuracy of r_{bg} measured in a transmission experiment.

2 Iterative method

Here we introduce an iterative approach to handle X-ray scattering background and derive the scaling factor. This method is based on the assumption that the theoretical model used to interpret the scattering data can correctly represent the underlying physical structure of a sample. Thus, a scattering curve, calculated using a theoretical model to fit the experimental data with small divergence, gives a good interpretation to the data. And the ratio between the scattering intensities of any two points on the calculated and measured curves with the same wavevector transfer (q) values will be essentially the same. Our method applies this principle in a more effective way. Due to background noise, experimental data always show fluctuations, so instead of calculating the ratio between single data points, we take ratio of the averaged values of neighboring points. In practice, three points at low q usually with good signal-to-noise ratio, and three points at high q without fast changing features like oscillations, are taken into account. We find that the mean of three data points is sufficient for the present study, while more points are required for experimental data with low signal-to-noise ratios in order to attain reliable results.

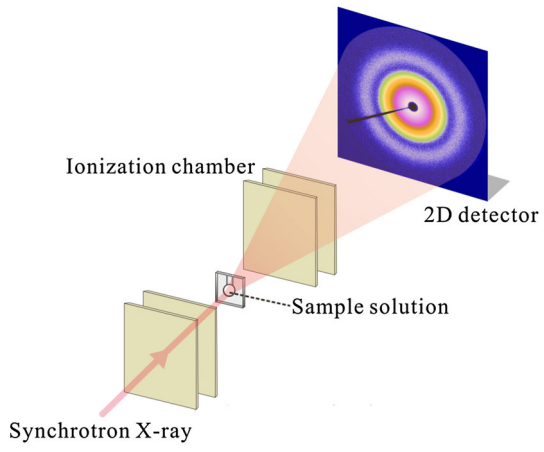

Fig. 1 Typical X-ray scattering setup with the sample positioned between two ionization chambers, and an area detector to record the scattering

First, we compute the ratio r_{hl} of the averaged values for the theoretical scattering curve,

$$r_{hl} = I_{calc}(h3)/I_{calc}(l3), \quad (2)$$

where $I_{calc}(h3)$ and $I_{calc}(l3)$ are average values of three data points at high and low q values, respectively. Assuming the theoretical curve gives a good fit to the experimental data, one can write

$$r_{hl} = I_s(h3)/I_s(l3) = [I_{sb}(h3) - r_{bg} I_b(h3)]/[I_{sb}(l3) - r_{bg} I_b(l3)], \quad (3)$$

where $I_s(h3)$ and $I_s(l3)$ are average values of three points at high and low q of the net scattering curve, respectively. Substituting Eq. (2) into Eq. (3), the scaling factor r_{bg} can be obtained,

$$r_{bg} = [I_{calc}(l3) I_{sb}(h3) - I_{calc}(h3) I_{sb}(l3)]/[I_{calc}(l3) I_b(h3) - I_{calc}(h3) I_b(l3)]. \quad (4)$$

The net scattering signal, I_s, can be obtained by substituting r_{bg} into Eq. (1). This method can automatically separate scattering signal from background in the data fitting process and requires no ionization chamber readings, hence no parasitic scatterings nor influence of incident beam fluctuations. The selection of a suitable theoretical model to fit experimental data is essential for this method. Any poor interpretation to the sample structure will lead to unacceptable results. Recently, this method was applied successfully to the structural reconstruction of Pt-coated Au dumbbells [15] and Au plasmonic nanostructures [16].

3 Experimental and theoretical considerations

To validate the feasibility of the iterative background subtraction method we proposed, small angle X-ray scattering (SAXS) experiments were carried out on Beamline BL16B1 [17] of Shanghai Synchrotron Radiation Facility (SSRF). Two types of Au nanoparticles in small (Sample-S) and large (Sample-L) diameters were dispersed in a solution and measured separately with the incident X-ray beams at 10 keV, using an MAR165 area detector.

X-ray scattering amplitude from a sphere can be written as [18, 19]

$$F(q) = (4/3)\pi r_e \rho r^3 \Phi(qr), \quad (5)$$

where r_e is the Thomson scattering length, ρ is the electron density difference between gold nanospheres and the

solvent, r is the radius of gold nanospheres, and the $\Phi(x)$ function stands for

$$\Phi(x) = 3(\sin x - x \cos x)/x^3, \tag{6}$$

The detectable X-ray scattering intensity, $I(q)$, is a total summation of the modulus square of $F(q)$ multiplied by their corresponding statistical probability due to the size distribution of nanospheres,

$$I(q) = \int |F(q)|^2 G(r)\, \mathrm{d}r, \tag{7}$$

where $G(r) = \exp[-(r-\mu)^2/(2\sigma^2)]/[\sigma(2\pi)^{1/2}]$ is the Gaussian distribution of the nanospheres radius r with two variables of the mean value μ and the standard deviation σ.

In the fitting process, a target function J to assess the similarity between the experimental net scattering intensity $I_s(q)$ and the calculated intensity $I_{calc}(q)$ is given as

$$J = 1 - \left| \frac{\sum_q \left[I_s(q) - \overline{I_s(q)}\right]\left[I_{calc}(q) - \overline{I_{calc}(q)}\right]}{\sqrt{\sum_q \left[I_s(q) - \overline{I_s(q)}\right]^2 \sum_q \left[I_{calc}(q) - \overline{I_{calc}(q)}\right]^2}} \right|, \tag{8}$$

where the second term is the absolute value of normalized cross-correlation [20] and the over bar denotes the average. The J function has a range from 0 to 1, where "1" refers to no linear correlation, while "0" to a strong linear proportional correlation or a perfect fit for the calculated and experimental data. A global optimization algorithm called covariance matrix adaptation evolution strategy (CMAES) [21] was applied to optimize the model parameters. There are two fitting parameters μ and σ for conventional and iterative methods.

4 Results and discussion

The fitting results for Sample-S and Sample-L are shown in Fig. 2 with their parameters listed in Table 1. For Sample-S, the J function values obtained by the iterative method about six times smaller than that from the conventional method (Table 1), implying that structural parameters obtained from the iterative method provide much better interpretations to the data than the conventional method (Fig. 2a). For the conventional method, the theoretical scattering curve deviates for $q > 1.15$ nm^{-1} from the experimental data, though they fit well for $q \leq 1.15$ nm^{-1}. So, the ascribed $r_{bg} = 0.99$ in Table 1, obtained conventionally, is inaccurate. It has a strong influence for data points at large q values, because at this region, I_b and I_{sb} have the same magnitude and any small change to r_{bg} will make a big difference on the final data curve. For sample-L, the values of J and r_{bg} obtained by

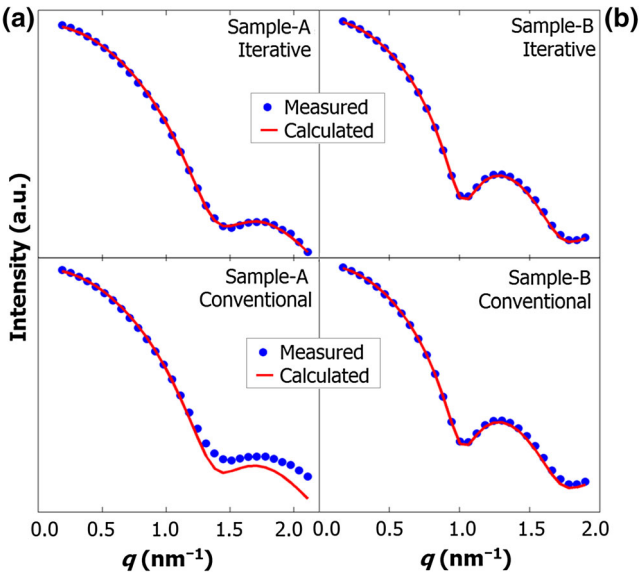

Fig. 2 Comparison of two scattering background subtraction methods used in SAXS data fittings

both methods are close to each other, and the theoretical and experimental scattering curves are in good agreement (Fig. 2b). These results demonstrate that the iterative method is effective in handling SAXS background, particularly for data points at high q region. In contrast, the conventional method is not always valid, because r_{bg} obtained directly from ionization chamber readings may be unreliable.

In Fig. 3, the particle size distributions of the two samples obtained by SAXS measurements, using the two background subtraction methods, are compared with the transmission electron microscopy (TEM) results. Some parts of the TEM images of Sample-S and Sample-L are depicted in the insets of Fig. 3. For Sample-S, the mean radius and standard deviation are 3.06 and 0.41 nm as obtained from the Gaussian fit to the TEM distribution histogram. As shown in Fig. 3a, the particle size distributions by the iterative method agree better with the Gaussian fit from the TEM data than the conventionally obtained particle size distributions, which shift slightly toward larger radii. For Sample-L, the mean radius is (4.33 ± 0.38) nm as obtained from the Gaussian fit to the TEM data. The particle size distributions derived from both methods agree very well with the Gaussian fit obtained from the TEM histogram as shown in Fig. 3b. The details of the particle structural parameters are summarized in Table 1.

Next, the influence of scaling factor deviation from a proper value on the final fitting results is demonstrated with Sample-S. The fitting results with the scaling factor increased by 5 % (r_{bg}^{i5}) and 10 % (r_{bg}^{i10}), and decreased by 5 % (r_{bg}^{d5}) and 10 % (r_{bg}^{d10}), with respect to the value obtained from the iterative method (r_{bg}^{IM}) shown in Fig. 4.

Table 1 Mean radii (μ), standard deviations (σ), scaling factor r_{bg} and target function J, obtained by different methods

Methods	Sample-S				Sample-L			
	μ_S (nm)	σ_S (nm)	r_{bg}	J ($\times 10^{-4}$)	μ_L (nm)	σ_L (nm)	r_{bg}	J ($\times 10^{-5}$)
TEM fitting	3.06	0.41	–	–	4.33	0.38	–	–
Iterative	3.06	0.42	1.06	1.54	4.35	0.38	1.12	6.11
Conventional	3.10	0.41	0.99	9.72	4.35	0.39	1.11	5.71

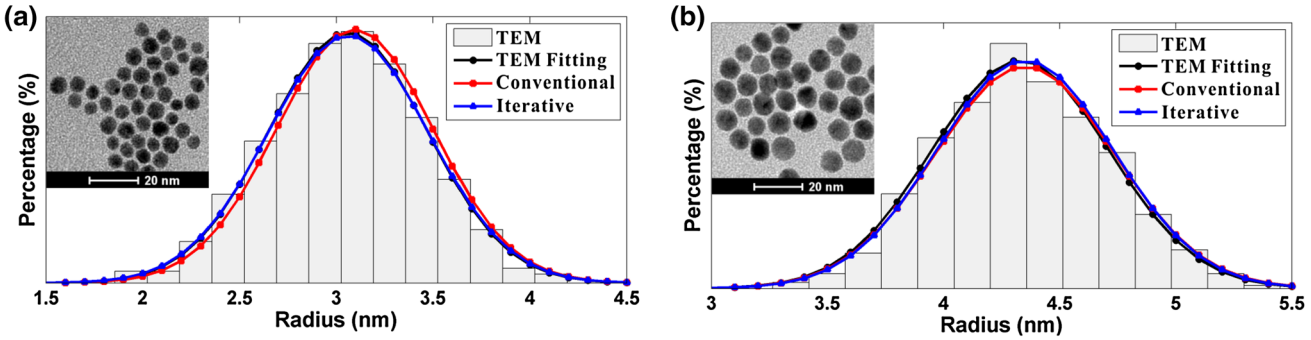

Fig. 3 Comparison of the Au NP size distributions obtained from TEM measurements and SAXS data fittings using different background subtraction methods for Sample-S (**a**) and Sample-L (**b**). The *insets* show parts of TEM images of two types of Au NPs

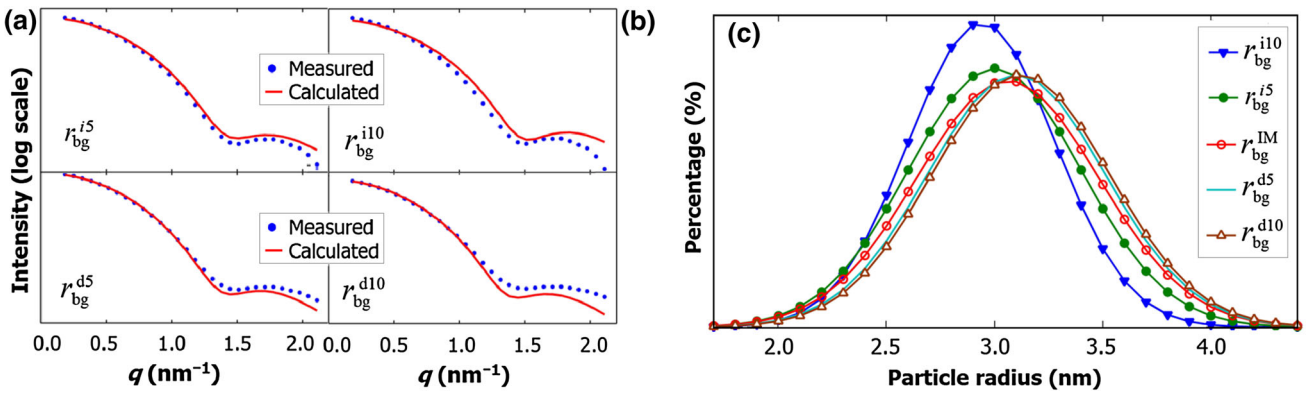

Fig. 4 Fitting results for Sample-S with the scaling factor altered by 5 % (**a**) and 10 % (**b**) with respect to the value obtained from our method. The experimental and theoretical data are plotted with *blue dots* and *red lines*, respectively. **c** Particle size distributions of Sample-S obtained using different scaling factors for background subtraction. (Color figure online)

Using r_{bg}^{i5} and r_{bg}^{d5}, the J function values are about fivefold than those obtained from r_{bg}^{IM}, and the fits are not satisfactory (Fig. 4a). For r_{bg}^{i10} and r_{bg}^{d10}, the J function values become even larger, and the fittings are not acceptable. Especially for r_{bg}^{i10}, the net scattering intensity drops sharply at the large q values (Fig. 4b) due to a large scaling factor being used to subtract the scattering background. The particle size distributions obtained using the four scaling factors are shown in Fig. 4c. It can be seen that the particle radii obtained with r_{bg}^{d5} and r_{bg}^{d10} shift slightly toward large values as compared to those from r_{bg}^{IM}. For r_{bg}^{i5} and r_{bg}^{i10}, the particle radii shift toward smaller values, especially for r_{bg}^{i10}. As summarized in Table 2, the results clearly illustrate on a simple system the importance of accurate determination of the scaling factor for SAXS background subtraction. The net scattering intensities depend sensitively on the scaling factor especially at high q regions, and any slight deviation from an adequate value would significantly affect the final results.

Table 2 Structural parameters obtained for Sample-S using different scaling factors to subtract scattering background

Scaling factors	μ_S (nm)	σ_S (nm)	J ($\times 10^{-3}$)
r_{bg}^{i5}	3.00	0.40	0.87
r_{bg}^{d5}	3.10	0.41	0.69
r_{bg}^{i10}	2.94	0.34	5.47
r_{bg}^{d10}	3.12	0.41	1.53

5 Conclusion

In summary, we have proposed an iterative X-ray scattering background subtraction method with its feasibility and reliability demonstrated by SAXS studies of Au NPs. It is better than conventional method in fittings the experimental data in good agreements with the TEM results. Also, the influence of the scaling factor deviation on the final results is examined. While we demonstrate in the present study the validation of the iterative method to the Au nanoparticle model system, it has been successfully applied to the structural reconstructions of Pt-coated Au dumbbells [15] and Au plasmonic nanostructures [16]. In contrast to the microscopic techniques such as TEM where an object or a small part of the sample is magnified and investigated, for X-ray scattering the whole illuminated sample volume is studied and consequently the averaged structural parameters are obtained. For an unknown sample, both methods are required in order to capture a complete picture as they are complementary to one another. Moreover, X-rays can penetrate through gas, liquid and solid, which makes them ideal sources to carry out in situ measurements with specimens in their natural environments. Whereas it is certainly advantageous to explore sample properties under their genuine conditions, the surrounding media would bring additional scattering background and any miscalculation can render the final results unreliable. In this regard, the iterative method provides an effective way to handle X-ray scattering background and can be generally applied to a variety of scattering experiments. It will not only be beneficial to studying samples in gas or liquid environments but also resolving weak scatterings from samples like surfactant and polymer micelles and biological proteins.

Acknowledgments We thank all the team members at BL16B1 of SSRF.

References

1. G.L. Hura, A.L. Menon, M. Hammel et al., Robust, high-throughput solution structural analyses by small angle X-ray scattering (SAXS). Nat. Methods **6**, 606–612 (2009). doi:10.1038/nmeth.1353
2. H.D.T. Mertens, D.I. Svergun, Structural characterization of proteins and complexes using small-angle X-ray solution scattering. J. Struct. Biol. **172**, 128–141 (2010). doi:10.1016/j.jsb.2010.06.012
3. D. Nykypanchuk, M.M. Maye, D. Lelie et al., DNA-guided crystallization of colloidal nanoparticles. Nature **451**, 549–552 (2008). doi:10.1038/nature06560
4. T. Wang, J. Zhuang, J. Lynch et al., Self-assembled colloidal superparticles from nanorods. Science **338**, 358–363 (2012). doi:10.1126/science.1224221
5. S.V. Roth, T. Autenrieth, G. Grübel et al., In situ observation of nanoparticle ordering at the air-water-substrate boundary in colloidal solutions using x-ray nanobeams. Appl. Phys. Lett. **91**, 091915 (2007). doi:10.1063/1.2776850
6. S. Humbert, O. Lame, J.M. Chenal et al., New insight on initiation of cavitation in semicrystalline polymers: in-situ SAXS measurements. Macromolecules **43**, 7212–7221 (2010). doi:10.1021/ma101042d
7. M.K. Crawford, R.J. Smalley, G. Cohen et al., Chain conformation in polymer nanocomposites with uniformly dispersed nanoparticles. Phys. Rev. Lett. **110**, 196001 (2013). doi:10.1103/PhysRevLett.110.196001
8. W. Hayes, R. Loudon, *Scattering of Light by Crystals* (Dover, New York, 2004)
9. T. Zemb, P. Lindner, *Neutrons, X-rays and Light: Scattering Methods Applied to Soft Condensed Matter* (North-Holland, Amsterdam, 2002), pp. 23–48
10. H. Schnablegger, Y. Singh, in *The SAXS Guide: Getting acquainted with the principles* (Anton Paar GmbH, Austria, 2011), pp. 45–47
11. T. Morita, K. Kusano, H. Ochiai et al., Study of inhomogeneity of supercritical water by small-angle X-ray scattering. J. Chem. Phys. **112**, 4203–4211 (2000). doi:10.1063/1.480965
12. T. Wolff, C. Burger, W. Ruland, Synchrotron SAXS study of the microphase separation transition in diblock copolymers. Macromolecules **26**, 1707–1711 (1993). doi:10.1021/ma00059a033
13. Y. Kasahara, K. Nishikawa, Construction of small-angle X-ray scattering diffractometer using asymmetric channel-cut monochromator. Jpn. J. Appl. Phys. **39**, 343–344 (2000). doi:10.1143/JJAP.39.343
14. B.R. Pauw, Everything SAXS: small-angle scattering pattern collection and correction. J. Phys. Condens. Matter **25**, 383201 (2013). doi:10.1088/0953-8984/26/23/239501
15. G. Chen, M.A. Modestino, B.K. Poon et al., Structure determination of Pt-coated Au dumbbells via fluctuation X-scattering. J. Synchrotron Radiat. **19**, 695–700 (2012). doi:10.1107/S0909049512023801
16. J. Shen, L. Xu, C. Wang et al., Dynamic and quantitative control of the DNA-mediated growth of gold plasmonic nanostructures. Angew. Chem. Int. Ed. **53**, 8338–8342 (2014). doi:10.1002/anie.201402937
17. F. Tian, X.-H. Li, Y.-Z. Wang et al., Small angle X-ray scattering beamline at SSRF. Nucl. Sci. Tech. **26**, 030101 (2015). doi:10.13538/j.1001-8042/nst.26.030101
18. A. Guinier, G. Fournet, *Small-Angle Scattering of X-rays* (Wiley, New York, 1955)
19. O. Glatter, O. Kratky, *Small Angle X-ray Scattering* (Academic, London, 1982)
20. G. Chen, P.H. Zwart, D. Li, Component particle structure in heterogeneous disordered ensembles extracted from high-throughput fluctuation X-ray scattering. Phys. Rev. Lett. **110**, 195501 (2013). doi:10.1103/PhysRevLett.110.195501
21. N. Hansen, A. Ostermeier, Completely derandomized self-adaptation in evolution strategies. Evol. Comput. **9**, 159–195 (2001). doi:10.1162/106365601750190398